Surface Electric Fields Increase Osteoblast Adhesion through Improved Wettability on Hydroxyapatite Electret

Miho Nakamura,*,† Akiko Nagai,† Teuvo Hentunen,‡ Jukka Salonen,‡ Yasutaka Sekijima,† Toshinori Okura,§ Kazuaki Hashimoto,|| Yoshitomo Toda,|| Hideki Monma,§ and Kimihiro Yamashita†

Institute of Biomaterials and Bioengineering, Tokyo Medical and Dental University, 2-3-10 Kanda-Surugadai, Chiyoda, Tokyo 1010062, Japan, Department of Cell Biology and Anatomy, Institute of Biomedicine, University of Turku, Kiinamyllynkatu 10, 20520 Turku, Finland, Department of Environmental and Energy Chemistry, Kogakuin University, 2665-1 Nakano-cho Hachioji-shi, Tokyo 1920015, Japan, and Department of Life and Environmental Science, Chiba Institute of Technology, 2-17-1 Tsudanuma, Narashino, Chiba 2750016, Japan

ABSTRACT Osteoblasts are susceptible to the surface characteristics of bioceramics and stimulation from outside the cells. The purpose of this study was to evaluate the effects of electrical polarization on surface characteristics and osteoblastic adhesion. The surface characteristics revealed that electrical polarization had no effect on the surface roughness, crystallinity, and constituent elements. According to contact-angle measurements, electrically polarized hydroxyapatite (HA), which provides two kinds of surfaces, negatively charged HA (N-HA) and positively charged HA (P-HA), was even more hydrophilic than that of normal HA (O-HA). Morphological observations and quantitative analyses revealed that the typical adhered cells had a round shape on O-HA but had a spindle or fanlike spreading configuration on N-HA and P-HA 1 h after seeding. After 3 h of cultivation, the rate of the number of spread cells and the size of the focal adhesions on O-HA increased and approached that of N-HA and P-HA. However, the cell areas positively stained for actin, which indicates the degree of cell spreading, were distinctly larger on N-HA and P-HA than that on O-HA. The number of focal adhesions per cell was also less than that on N-HA and P-HA.

KEYWORDS: cell adhesion • cell spreading • hydroxyapatite • osteoblast • wettability

INTRODUCTION

Numerous studies on an interface between inorganic biomaterials and cells have been carried out for control of the osteoblast behavior including adhesion, proliferation, and differentiation. Control of the osteoblast behavior contributes to improved osteoconductivity, which is the formation of new bone in the vicinity of the implanted biomaterials. Generally, adhesion of the osteoblasts to inorganic biomaterials plays a predominant role in the regulation of the subsequent differentiation and formation of the extracellular matrix following spreading and motility (1). Adhesion of the osteoblasts is primarily the result of two subjects, namely, the surface characteristics of the biomaterials involved and stimulation from outside the cells. The former subject, surface characteristics, including the topography, constituent elements, functional group, and wettability of biomaterials affect osteoblast attachment and adhesion (2−5). The surface characteristics were reportedly affected by the surface roughness, surface crystallinity (2−4), constituent elements at the surface, and incorporation of ions such as carbonate or fluorine (6, 7). In addition, electron-induced surface-energy modifications such as photoluminescence and surface photovoltage spectroscopy were also effective in the improvement of the surface characteristics (8). The latter subject, stimulation from outside the cells, which includes electrical stimulation such as capacitive coupling, inductive coupling, and combined electromagnetic fields, affects osteoblast attachment, adhesion, and motility (8).

The mechanism of cell adhesion on biomaterials varies according to the type of substrate. Human osteoblast-like cells initially attached and spread more quickly on hydroxyapatite (HA) than on titanium (1). HA and titanium surfaces, furthermore, influence gene expression at an early phase of adhesion as well as at the later phases of proliferation and differentiation (4). These behaviors of osteoblasts can be attributed to the differences in surface characteristics because the differences affect the signal transduction pathways. The signal transduction pathways involved in the adhesion of osteoblasts on HA and titanium were confirmed by the subsequential expression of $\alpha_v\beta_1$ integrins (1).

Cell shapes on substrates are dependent on the integrin-mediated cytoskeletal and signal transduction molecules,

* To whom correspondence should be addressed. Phone: +81-3- 5280-8015. Fax: +81-3-5280-8013. E-mail: miho.bcr@tmd.ac.jp.
Received for review May 18, 2009 and accepted August 27, 2009
† Tokyo Medical and Dental University. E-mail: nag.bcr@tmd.ac.jp (A.N.), ys-27-ys@dc4.so-net.ne.jp (Y.S.); yama-k.bcr@tmd.ac.jp (K.Y.).

‡ University of Turku. E-mail: teuhen@utu.fi (T.H.), jusalon@utu.fi (J.S.).

§ Kogakuin University. E-mail: okura@cc.kogakuin.ac.jp (T.O.), monma@cc.kogakuin.ac.jp (H.M.).

|| Chiba Institute of Technology. E-mail: kazuaki.hashimoto@it-chiba.ac.jp (K.H.), toda.yoshitomo@it-chiba.ac.jp (Y.T.).

DOI: 10.1021/am900341v

such as actin filaments and vinculin (9, 10), and are important during cell−substrate adhesion for subsequent cell behaviors such as proliferation and differentiation (7, 11). Vinculin molecules are involved in the cytoplasmic domain of focal adhesion and seem to be responsible for transmitting signals from integrins on the cell surface to cytoskeletal actin filaments by the formation of focal adhesions. Because cell adhesion that is mediated via focal adhesions undergoes dynamic changes in the structure and molecular properties from dotlike focal complexes to matured focal contacts, the number, size, and localization in the adhered cells are important (11). Therefore, we concentrated on the adhered cell shapes that were indicated by the actin structure and vinculin localization in order to study osteoblast adhesion.

We have recently demonstrated that the charged surfaces on HA (12−16) were induced by polarization-enhanced osteoconductive capabilities (17, 18) *in vivo*. The new bone formation and localization of the osteoblasts positively stained for alkaline phophatase were enhanced in the center of the polarized porous HA specimens after 3 weeks of implantation into the tibiae of rabbits compared with the conventional porous HA specimens (18). The polarized HA also accelerated protein adsorption at an early stage after implantation (19). The adsorption of fibrin protein was accelerated on the polarized HA after 5 min of implantation into the tibiae of rats compared with the conventional dense HA specimens. Additionally, the polarized HA had effects not only on the hard tissues but also on the soft tissues. The polarized HA enhanced the blood vessel regeneration of a vascularly injured model (20) and epidermal recovery from full-thickness skin wounds *in vivo* (21). On the basis of the aforementioned results of the enhancement of tissue regeneration of both hard and soft tissues *in vivo*, the polarization treatment is considered to have effects on cell behaviors. The initial adhesion and motility of osteoblast-like cells (MC3T3-E1 osteoblast cell line) were accelerated *in vitro* (22). Although the polarization treatment enhanced behaviors of the osteoblast cell line *in vitro*, the mechanisms of the effects induced by the polarization treatment on the osteoblast behavior were not completely recognized. Considering two important subjects in cell adhesion, including the surface characteristics of the materials and stimulation from outside the cells, we focused on the surface characteristics of polarized HA and the effects of electrical stimulation by polarization on primary osteoblast behavior *in vitro* in order to study the mechanism of the effects of enhancement.

MATERIALS AND METHODS

Surface Characteristics. The HA powder was synthesized from the analytical-grade reagents of calcium hydroxide and phosphoric acid by the wet method (15). The HA powder was calcined at 850 °C and pressed into a mold at 200 MPa. In order to suppress dehydration, the HA compacts were sintered in a saturated water vapor atmosphere at 1250 °C for 2 h. The sintered HA specimens were electrically polarized according to our previous work (15) with a pair of platinum electrodes at 400 °C in direct-current (dc) electric fields of 5 kV/cm for 1 h in air.

X-ray diffraction (XRD) measurements of the normal HA (O-HA), the negatively charged HA (N-HA), and the positively charged HA (P-HA) surfaces were performed for phase analysis at room temperature (RT) with Cu Kα radiation at 40 kV and 40 mA on a Philips PW1700 diffraction spectrometer equipped with a graphite monochromator. X-ray photoelectron spectroscopy (XPS) analysis was performed for compositional analysis using a Scienta ESCA 200 spectrometer (Sweden) with Al Kα X-rays under an analytical angle of 45°.

Polarization of the HA specimens was verified by thermally stimulated depolarization current (TSDC) measurement before and after cell cultivation. The TSDC measurements were carried out according to our previous study (14, 15) in air from RT to 600 °C at a heating rate of 5.0 °C/min. The depolarization current was measured with a Hewlett-Packard 4140B pA meter. The values of the polarization charge (Q_p) were calculated from the TSDC spectra using the equation

$$Q_p = 1/\beta \int J(T)\, dT$$

where $J(T)$ is the measured dissipation current density at temperature T and β is the heating rate.

Wettability Analysis. The surface roughnesses of O-HA, N-HA, and P-HA were analyzed using a laser microscope (Keyence, VK8500). A total of 15 measurements on each specimen were performed to obtain an average. Specimens with an average density of 98% and an R_a value of 0.05 were used for contact-angle measurements.

The highly crystalline HA specimens were electrically polarized with a pair of platinum electrodes under two sets of conditions. One was the mild condition at 400 °C in dc electric fields of 5 kV/cm for 1 h in air [1]. The other was the strong condition at 550 °C in dc electric fields of 10 kV/cm for 6 h in air [2]. The unpolarized normal HA was designated as O-HA as the control. The N-HA polarized under conditions [1] and [2] were designated as N-HA(400) and N-HA(550), respectively. The P-HA polarized under conditions [1] and [2] were designated P-HA(400) and P-HA(550), respectively.

Contact-angle measurements were performed on the O-HA, N-HA, and P-HA specimens using distilled and deionized water (Kyowa Interface Science, DropMaster DM-500). Contact angles were calculated by Young's equation:

$$\gamma_{SV} = \gamma_{LV} \cos\theta + \gamma_{SL}$$

where subscripts S, L, and V refer to solid, liquid, and vapor. A total 10 measurements on each specimen were performed, and independent experiments were conducted on three different specimens. The average values of the O-HA, N-HA, and P-HA from 10 measurements each were determined. A one-way ANOVA test was performed to determine the statistical significance ($p < 0.05$) of the differences in the values of wettability as well as surface topography.

Cell Adhesion Assay. Mouse mesenchymal stem cells were isolated from the tibiae and femurs of C57Bl/6J mice (female, 8−12-week-old) as described in detail (23). Briefly, the mice were euthanized and sterilized with 70% ethanol. Soft tissues were removed, and the tibiae and femurs were separated. The epiphyses were resected, and bone marrow cells were flushed out with α-modified essential Medium (α-MEM) including 10% heat-inactivated fetal calf serum (FCS), 100 IU/mL penicillin, and 100 μg/mL streptomycin using a syringe and a needle. Nucleated cells were counted in a hemocytometer; the cells were dispersed at a density of 1×10^6 cells/cm^2. The cells were maintained for 7 days in an osteoinductive culture medium, α-MEM, including 15% FCS, 100 IU/mL penicillin, 100 μg/mL streptomycin, 10 nM dexamethasone, 50 μg/mL ascorbic acid,

Table 1. Average Values of the Relative Densities and the Surface Roughness (R_a) of Sintered Dense HA Specimens[a]

	O-HA	N-HA	P-HA
relative density (%)	98	98	98
surface roughness (Ra)	0.5 ± 0.01	0.5 ± 0.01	0.5 ± 0.01

[a] The R_a values were measured using a laser microscope. No significant differences in the relative densities and R_a were found among O-HA, N-HA, and P-HA.

and 10 mM sodium β-glycerophosphate in a humidified atmosphere of 95% air and 5% CO_2 at 37 °C.

The adherent cells were scraped and centrifuged at 1000 rpm for 5 min. The supernatant was removed, and the cell pellet was suspended in the culture medium. The cells were seeded at a density of 1×10^4 cells onto the HA specimens, which were sterilized with 70% ethanol, and immersed in the culture medium for 30 min. At 1 and 3 h after seeding, the cells on the HA surfaces were fixed with 4% paraformaldehyde and blocked with 5% goat serum in 0.1% Triton X-100 in phosphate-buffered saline (PBS). The primary antibody in the blocking solution was added for 1 h at RT. Following extensive washing with PBS, the HA specimens were incubated in Alexa-conjugated goat immunoglobulin in a blocking solution containing rhodamine phalloidin for 1 h at RT. After 4,6-diamino-2-phenylindole staining, fluorescent signals were observed using a fluorescence microscope (Olympus IX71).

From the fluorescence actin staining, the cell morphology was categorized into three types: round, semispread, and well-spread (24). The first category, round, shows the cells just attached with a circular or spherical shape. The second category, semispread, shows the cells slightly spread with no stress fiber or lamellipodia structure. The third category, well spread, shows the cells with stress fiber or lamellipodia structure. The categorization was performed for a minimum of 80 cells on each surface. In addition, the cell areas positively stained for actin were measured using *MetaMorph* software. The measurement was performed for a minimum of 50 cells on each surface. From the fluorescence vinculin staining, the number per cell and the size of the vinculin-positive focal adhesions were measured using *MetaMorph* software. The measurement was performed for a minimum of 50 cells on each surface.

Accurate quantification in five different HA specimens was achieved by three independent experiments. The differences between the two groups were analyzed using one-way or two-way analysis of variance (ANOVA). The Student's *t* test (paired or unpaired) was used to ascertain the differences between the two groups. The statistical significance was defined as $p < 0.05$.

RESULTS

Both the density and surface roughness (R_a) of the employed HA specimens are summarized in Table 1, indicating their relative densities of 98% and average R_a values of 0.5 ± 0.02. No significant differences in the surface roughness were found among O-HA, N-HA, and P-HA. The XRD patterns of O-HA, N-HA, and P-HA were highly consistent with the published data of HA (JCPDS no. 9-432), indicating that the HA surfaces consisted of a single phase of hexagonal HA before and after polarization (Figure 1).

XPS survey-scan spectra of the O-HA, N-HA, and P-HA surfaces are shown in Figure 2A. By comparison with the published data of XPS spectra (25), no differences in the representative XPS spectra were found among O-HA, N-HA, and P-HA, indicating that no significant changes occurred in the elements on the XPS analytical level during polarization. Although the C 1s peak was observed in all of the

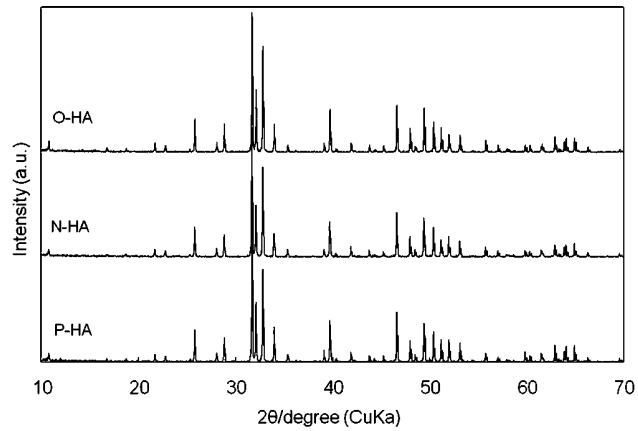

FIGURE 1. XRD patterns of O-HA, N-HA, and P-HA. The dense HA specimens sintered in a saturated water vapor atmosphere at 1250 °C for 2 h were polarized at 400 °C in dc fields of 5 kV/cm in air. The patterns were matched to the published data of HA (JCPDS no. 9-432) and demonstrated that the surfaces of the HA specimens consisted of a single phase of hexagonal HA.

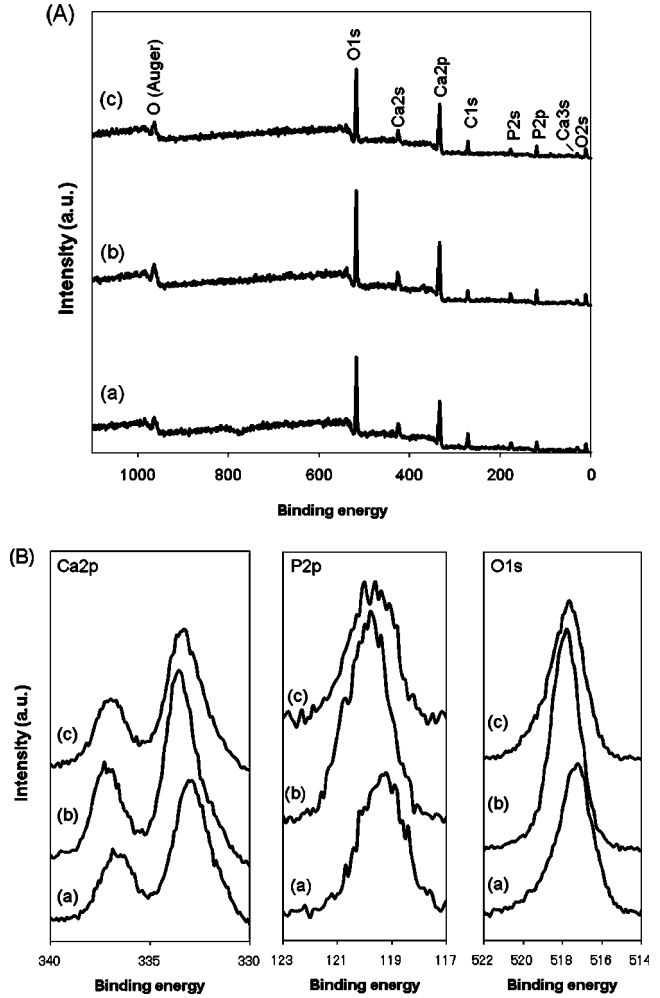

FIGURE 2. (A) Spectra of the XPS survey scan of O-HA (a), N-HA (b), and P-HA (c). The representative spectra show the peaks corresponding to the same s and p orbitals of oxygen, calcium, phosphorus, and carbon. (B) Spectra of the XPS detailed scan of O-HA (a), N-HA (b), and P-HA (c). The binding energies are 517 eV for oxygen, 347 and 351 eV for calcium, and 133 eV for phosphorus.

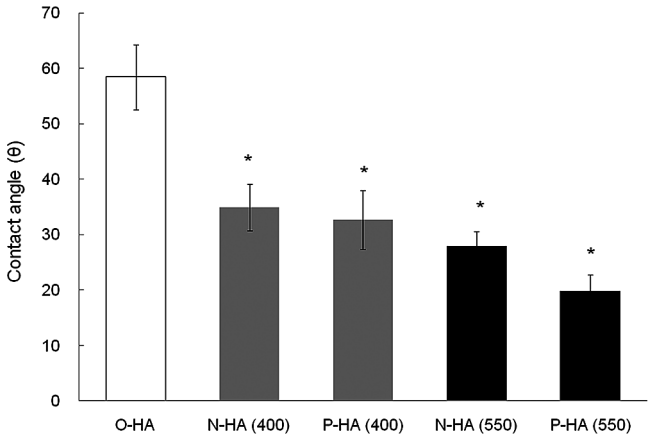

FIGURE 3. Contact-angle values of O-HA, N-HA (400 and 550), and P-HA (400 and 550) using distilled and deionized water. O-HA presented the highest values, indicating that the normal HA surface was a more hydrophobic material, while N-HA (400 and 550) and P-HA (400 and 550) presented a lower angle, being a more hydrophilic material.

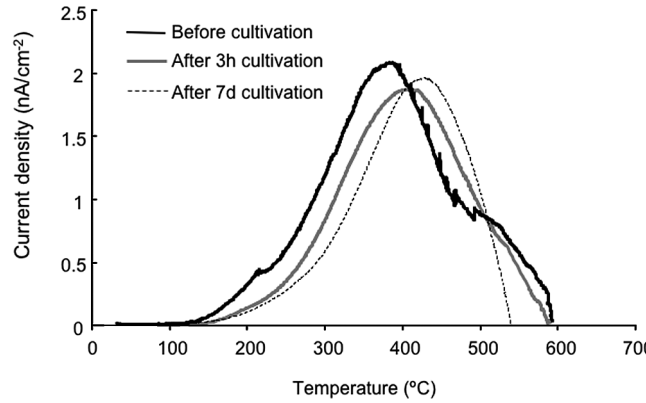

FIGURE 4. TSDC spectra of HA specimens retrieved from the culture medium compared with those of as-polarized HA. The lack of significant changes in the TSDC curves showed that the stored charges were estimated to be maintained during cell cultivation. Both of the TSDC curves before and after 3 h and 7 days of cell cultivation increased at ca. 150 °C and reached maximum points at ca. 400 °C and then gradually decreased. The stored charges were calculated from TSDC spectra at 5.2 μC/cm for before cultivation, at 4.6 μC/cm for after 3 h of cultivation, and at 4.0 μC/cm for after 7 days of cultivation, respectively.

specimens besides the expected calcium, phosphorus, and oxygen peaks, the carbon is the so-called adventitious carbon because of adsorption of the impurity hydrocarbon and generally has no effect on the interpretation for XPS measurements. The C 1s peak was used for calibration of the binding energies by setting its binding energy to 284.6 eV to correct for sample charging. Only peaks corresponding to some 1s and 2p orbital electrons of oxygen, calcium, phosphorus, and carbon were clearly observed on the XPS spectra of the HA surfaces. The binding energies are 517 eV for oxygen, 347 and 351 eV for calcium, and 133 eV for phosphorus (Figure 2B).

Figure 3 shows the contact-angle values obtained for the five different types of HA surfaces. O-HA presented the highest values, indicating that the normal HA surface was a more hydrophobic material, while N-HA (400 and 550) and P-HA (400 and 550) presented lower angles, thus being more hydrophilic. O-HA showed a contact angle of 60°, while N-HA (400) and P-HA (400) displayed a contact angle of 35°. N-HA (550) and P-HA (550) showed contact angles of 30° and 25°, respectively. These results indicated that the wettability improved on both N-HA and P-HA.

To evaluate whether polarization of HA was influenced during cell cultivation, the TSDC spectra of HA retrieved from the medium after 3 h and 7 days of cultivation were compared with those of as-polarized HA (Figure 4). Both of the TSDC curves of before and after cultivation increased at ca. 150 °C, reached maximum points at ca. 400 °C, and then gradually decreased. The stored charges (Q) from the TSDC spectra were calculated at 5.2 μC/cm for before cultivation, at 4.6 μC/cm for after 3 h of cultivation, and at 4.0 μC/cm for after 7 days of cultivation, respectively. As shown, there is no significant difference in the spectra, indicating that the stored charges were satisfactorily maintained on the HA surfaces during sterilization and cultivation.

Figure 5 shows vinculin, actin, and nuclei labeling of the cells after seeding onto the HA specimens for 1 h (A) and 3 h (B), respectively. Cytoskeletal organization and formation of focal adhesions on O-HA, N-HA, and P-HA were analyzed by immunofluorescence using antibodies directed against actin and vinculin. The majority of cells appeared to maintain a regular structure and presented a normal focal adhesion distribution.

During cultivation 1 h after cell seeding, the cells that adhered on O-HA showed a round or spherical configuration (Figure 5A). The localization of vinculin was equally observed in an accumulation of actin filaments in the round- or spherical-shaped cells on O-HA. The cells that adhered on N-HA (400 and 550) and P-HA (400 and 550) already showed a spindlelike or fanlike shape after 1 h of cultivation. As observed from the images of actin staining, the stress fiber formation was significantly stronger on N-HA (400 and 550) and P-HA (400 and 550) than on O-HA. Immunoreaction for vinculin was found in the peripheral regions of the cells that adhered on N-HA (400 and 550) and P-HA (400 and 550). Cells left for 1 h before fixing and staining on N-HA (400 and 550) and P-HA (400 and 550) had a well-spread shape and numerous focal adhesions scattered throughout their ventral surfaces. The distribution of vinculin-immunoreactive focal adhesions on N-HA (400 and 550) was similar to that of P-HA (400 and 550). Therefore, after 1 h of cultivation on N-HA (400 and 550) and P-HA (400 and 550), the differences of the polarization conditions had no obvious effects on the formation of the actin stress fiber or the focal contact distribution in the cells.

During subsequent incubation after 3 h of cell seeding, the cells that adhered on O-HA were spread and showed a slightly spindlelike or rectangular shape (Figure 5B). An accumulation of actin filaments in the periphery of lozenge-shaped cells was equally observed in N-HA (400 and 550) and P-HA (400 and 550). In addition, bundles of actin fibers forming stress fibers appeared in the cells on N-HA (400 and 550) and P-HA (400 and 550) as the attached cells spread. Well-defined stress fibers showing a regular arrangement with particular polarities were found in some cells grown on N-HA (400 and 550) and P-HA (400 and 550). In some cells

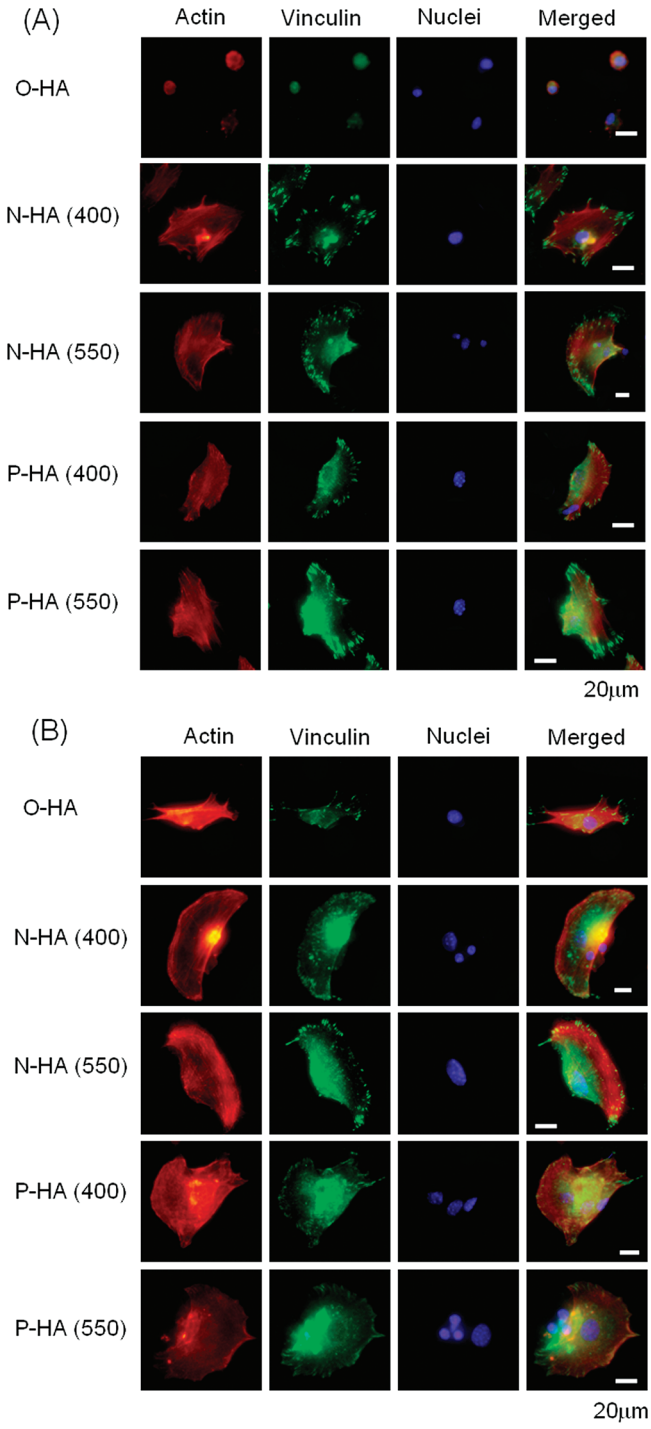

FIGURE 5. Morphology of the adhered osteoblastic cells on O-HA, N-HA, and P-HA. Actin, vinculin, nuclei, and merged fluorescence images of the cells cultured on the HA specimens for 1 h (A) and 3 h (B) are shown, respectively. (A) Actin staining showed round and spherical shapes and colocalization with vinculin on O-HA 1 h after seeding. However, the cells already showed a spindlelike or spread shape on N-HA and P-HA 1 h after seeding, as observed from the images of actin staining. Focal adhesions positively stained for vinculin were found in the peripheral regions of the cells on N-HA and P-HA. (B) During subsequent cultivation 3 h after seeding, the cells adhered on O-HA were elongated and showed a slightly spindlelike or rectangular shape. Vinculin-positive focal adhesions were found in the peripheral regions of the cells on O-HA. After 3 h of cultivation, an accumulation of actin filaments in the periphery of lozenge-shaped cells was observed in N-HA and P-HA. In addition, bundles of actin fibers forming stress fibers appeared in the cells as the attached cells spread. Vinculin-positive focal adhesions were found in the peripheral regions of the cells on N-HA and P-HA. Bar = 20 μm.

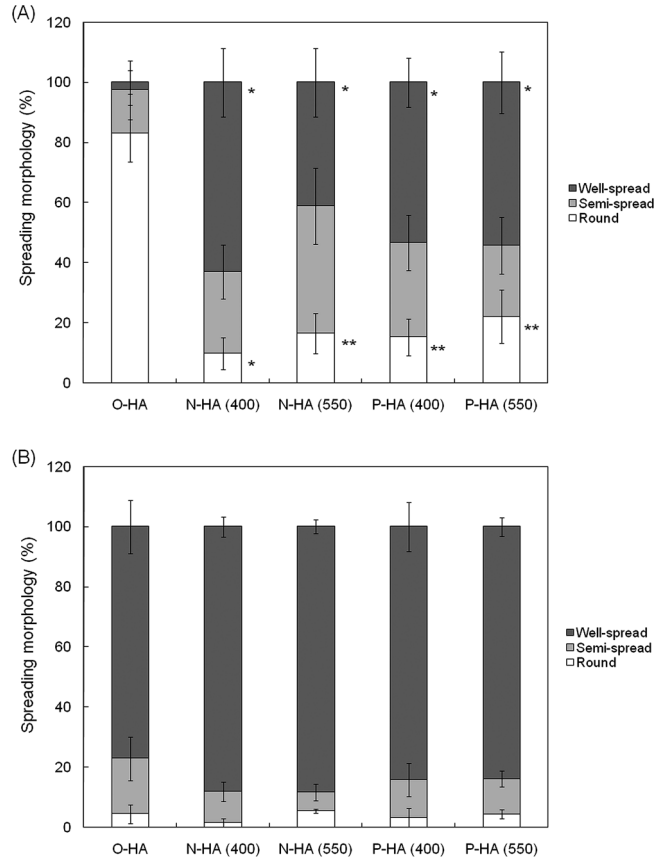

FIGURE 6. Cell morphologies after seeding were categorized into three types based on fluorescence actin staining. These were round, semispread, and well-spread. The first category of round shows the cells just attached with a circular or spherical shape. The second category of semispread shows the cells slightly spread with no stress fibers or lamellipodia structures. The third category of well-spread shows the cells with stress fibers or lamellipodia structures. (A) Categorization of the cells on the HA specimens 1 h after seeding. There was a remarkable difference in the cell spreading state between O-HA and the polarized HA, including N-HA (400 and 550) and P-HA (400 and 550) (* < 0.005 and ** < 0.02 compared with O-HA). (B) Categorization of the cells on the HA specimens 3 h after seeding. There was no significant difference between the cell spreading states of the five HA specimens.

on N-HA (400 and 550) and P-HA (400 and 550), the actin filaments were mostly distributed near the edge of pseudopodia-like structures and formed weak bundles of stress fibers. Immunoreaction for vinculin was found in the peripheral regions of the cells that adhered on O-HA, N-HA and P-HA (400 and 550). The distribution of vinculin-immunoreactive focal adhesions on N-HA (400 and 550) was similar to that of P-HA (400 and 550). Therefore, after 3 h of cultivation on N-HA (400 and 550) and P-HA (400 and 550), the differences of the polarization conditions had no obvious effects on the formation of the actin stress fiber or the focal contact distribution in the cells.

On the basis of fluorescence actin staining, the cell morphology was categorized into three types: round, semi-spread, and well-spread. There was a remarkable difference in the degree of spreading between O-HA and the polarized HA 1 h after seeding (Figure 6A). The rate of the cells categorized as round that were cultured on O-HA was 83%, while that on N-HA (400 and 550) and P-HA (400 and 550)

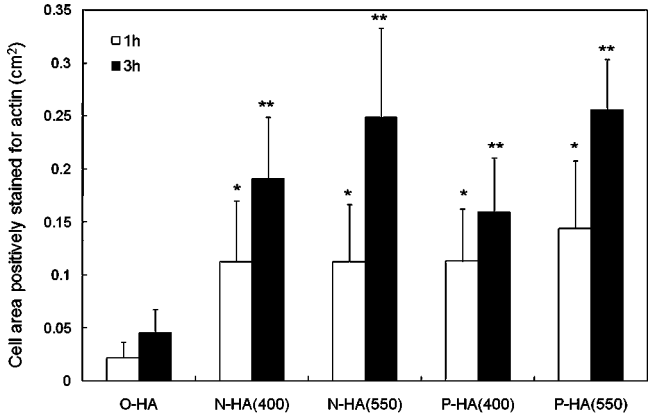

FIGURE 7. To quantify the degree of cell spreading between the five HA specimens, the cell areas positively stained for actin were measured using MetaMorph software. The cell areas increased from 1 to 3 h after seeding, which means that the cells spread and elongated on the HA specimens. The cell area was significantly larger on the N-HA (400 and 550) and P-HA (400 and 550), compared to the O-HA 1 h (* < 0.005 compared with O-HA) and 3 h (< 0.005 compared with O-HA) after seeding.**

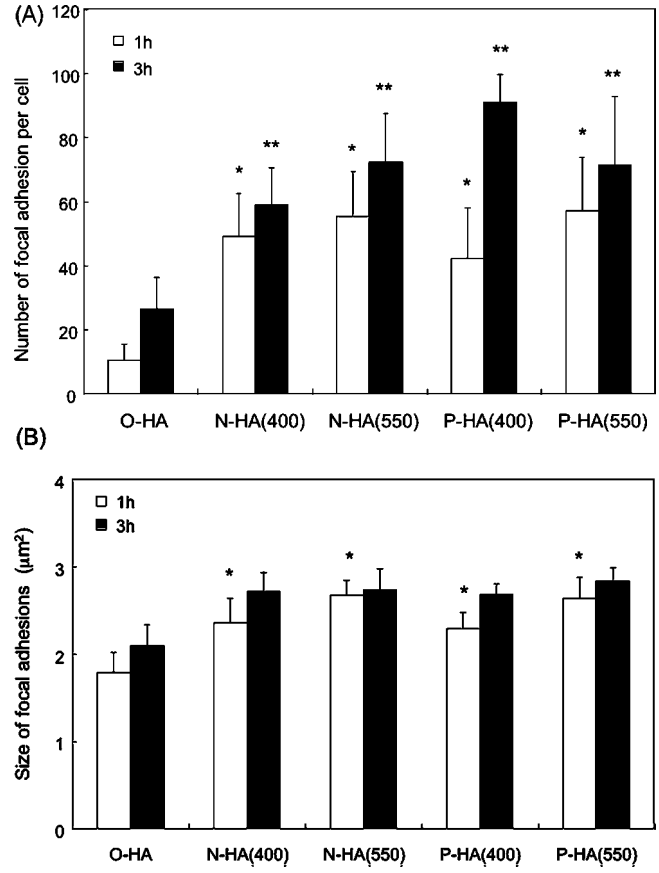

FIGURE 8. To quantify the formation of vinculin-positive focal adhesions between the five HA specimens, the number per cell (A) and the size (B) of focal adhesions were measured using *MetaMorph* software. (A) The number of focal adhesions per cell increased from 1 to 3 h after seeding, which means that the new focal adhesions were formed on HA specimens. The number of vinculin-positive focal adhesions was significantly larger on N-HA (400 and 550) and P-HA (400 and 550), compared to O-HA 1 h (* < 0.002 compared with O-HA) and 3 h (< 0.05 compared with O-HA) after seeding. (B) The size of focal adhesions slightly increased from 1 to 3 h after seeding, which means that the focal adhesions were matured on HA specimens. The size of the vinculin-positive focal adhesions was significantly larger on N-HA (400 and 550) and P-HA (400 and 550), compared to O-HA 1 h (* < 0.001 compared with O-HA) after seeding.**

was 10−22%. The cells categorized as semispread had almost equal subpopulations on every type of HA surface; the rate was 14−43%. The rate of the cells categorized as well-spread cultured on O-HA was 3%, while that on N-HA (400 and 550) and P-HA (400 and 550) was 41−63%. These results showed that the spread of the cells was accelerated on both N-HA and P-HA, compared with that on O-HA. The degree of spreading had no significant difference between the five HA specimens 3 h after seeding (Figure 6B). Although a few cells categorized as round (1−5%) or categorized as semispread (6−18%) still remained, most of the cells (77−88%) had well-spread morphologies on the five HA specimen types.

To quantify the difference in the degree of cell spreading between the five HA specimen types, the cell areas positively stained for actin that adhered were measured (Figure 7). The cell areas increased from 1 to 3 h, which means that the cells spread and elongated on the HA specimens. The cell areas were significantly larger on the N-HA (400 and 550) and P-HA (400 and 550), compared to the O-HA 1 and 3 h after seeding. The area of the cells cultured on the polarized HA was approximately five times or two times larger than the area on the O-HA 1 or 3 h after seeding, respectively. However, no significant differences in cell area were observed among the N-HA (400 and 550) and P-HA (400 and 550).

To quantify the difference in the formation of vinculin-positive focal adhesions between the five HA specimens, the number per cell and the size of the focal adhesions were measured (Figure 8). The number of focal adhesions per cell increased from 1 to 3 h after seeding, which means that the new focal adhesions were formed on HA specimens (Figure 8A). The number of vinculin-positive focal adhesions was significantly larger on N-HA (400 and 550) and P-HA (400 and 550) compared to O-HA 1 and 3 h after seeding. The size of the focal adhesions slightly increased from 1 to 3 h after seeding, which means that the focal adhesions were matured on HA specimens (Figure 8B). The size of the vinculin-positive focal adhesions was significantly larger on N-HA (400 and 550) and P-HA (400 and 550), compared to O-HA 1 h after seeding.

DISCUSSION

We have shown that the HA surface with its wettability improved by polarization affects the morphology of the adhered osteoblasts. An effect of polarization on wettability will be discussed here relative to conventional thoughts on the wettability of HA.

The measurement of the contact angle revealed that the wettability of the polarized HA was higher than that of O-HA, showing that both N-HA and P-HA were more hydrophilic than O-HA (Figure 3). Wettability has been reported to depend on the surface roughness or crystallinity on a solid surface (2−4). Considering these factors, the present study

employed HA specimens with almost equal surface roughness, crystallinity, and constituent elements at the surface, as shown in Table 1 and Figures 1 and 2. Thus, the improved wettability of the HA surfaces resulted from other factors. Modification of the surface wettability on HA was reportedly achieved by A-type carbonate apatite, corresponding to the location of the carbonate ions on monovalent anionic OH^- sites (6), and by fluoridated HA, incorporating fluorine in HA (7). However, improvement of the HA surface wettability by polarization did not affect the structural transformation. In contrast, electron-induced surface-energy modification such as photoluminescence and surface photovoltage spectroscopy was reported as an effective method of the surface-energy modification of the HA nanoparticle coating (8). The possible explanation for the improved surface wettability by polarization is the surface-energy modification because of the polar interaction energy with water.

The TSDC spectra before and after cultivation showed a similar diagram (Figure 4). The charges induced by polarization on the HA surfaces were maintained during immersion in 70% ethanol for sterilization and in a cell culture medium for 3 h and 7 days because the polarization occurred within the entire solid as a result of proton migration (15). This stability of the surface charges supported the idea that the effects by polarization were caused by the improved wettability during cell cultivation.

Morphological observation and quantitative analysis revealed that the typical adhered cells had a round or spherical shape on O-HA but had a spindle- or fanlike spreading configuration on N-HA (400 and 550) and P-HA (400 and 550) 1 h after seeding (Figures 5A and 6A). After 3 h of cultivation, the rate of the number of cells spreading on O-HA increased and approached that on N-HA and P-HA (Figures 5B and 6B). However, the cell areas positively stained for actin, which showed the degree of cell spreading on the HA specimens, were distinctly larger on N-HA and P-HA than on O-HA 1 and 3 h after seeding (Figure 7). These results demonstrated that the charges induced on the HA surfaces affected the percentages of the number of initial cells spreading against the total number of adhered cells and the degree of cell spreading on each cell.

Changes in the surface wettability of HA resulted from structural transformation and had effects on cellular behaviors. For example, A-type carbonate apatite and fluoridated HA affected cell proliferation and spreading, respectively (6). A-type carbonate apatite, corresponding to a location of carbonate ions at monovalent anionic OH^- sites, had lower wettability, lower cell spreading, and similar cell proliferation compared with HA. The incorporation of fluorine in HA caused an insignificant increase in the surface roughness and a slight increase in the contact angle (7). The fluoridated HA had no effect on the initial cell attachment but did have an effect on the cell spreading process. The surface wettability on several biomaterials other than apatite affects cell adhesion on the polymer (26), glass microscope slides (27), partially yttria-stabilized zirconia (28), poly(methyl methacrylate) (2), and titanium (3, 29). Despite the differences in the substrates or methods for the improvement of the surface wettability, changes in the surface wettability of biomaterials brought out advantages in cellular behaviors such as attachment and spreading. Therefore, the improvement of the surface wettability by polarization, consequently, contributed to the acceleration of cell spreading on N-HA (400 and 550) and P-HA (400 and 550). Whereas the improvement of the surface wettability, consequently, accelerated osteoblastic cell spreading, it had no effect on cell differentiation, especially mineralization (30, 31). It would be useful to further investigate whether the improvement in the surface wettability of HA by polarization affects the differentiation of osteoblastic cells.

The focal adhesions were highlighted by immunocytochemistry using mouse monoclonal antibodies against vinculin. Two types of cells stained for vinculin appeared. The first appearance of vinculin staining was observed in round and spherical cells, which approximately colocalized at nuclei and actin filaments. The second appearance of vinculin staining was observed in spread cells, which localized both at the cytoplasm with a dotlike structure and at the periphery with a larger spotlike structure. More than half of the cells on O-HA showed the first type of vinculin staining and had a small number and size of focal adhesion 1 h after seeding. On the other hand, almost all cells on N-HA (400 and 550) and P-HA (400 and 550) showed the second type of vinculin staining and had a large number and size of focal adhesion 1 h after seeding. When the cells were left for 3 h before fixing and staining, the majority of the cells on O-HA, N-HA, and P-HA showed the second type of vinculin staining and had matured large focal adhesion 3 h after seeding. Although the size of focal adhesions on O-HA was similar in N-HA (400 and 550) and P-HA (400 and 550), the number of focal adhesions per cell on O-HA was less than that on the polarized HA even after 3 h of cultivation.

The number, size, and localization of the vinculin-positive focal adhesions are important in adhered cells. Adhesions mediated via focal adhesions undergo dynamic changes in the actin structure and molecular properties from dotlike focal complexes to stress-fiber-associated focal contacts, which can further mature (11). In the first step of adhesion, small matrix adhesions denoted as focal complexes are formed. Focal complexes are short-lived structures, containing integrin and vinculin. They are early adhesions that transform into focal adhesions following the activation of RhoA or because of external mechanical perturbation (32). If stabilized, they will subsequently form focal adhesions, which can, in turn, transition to fibrillar adhesions (33). Excessive enlargement of focal adhesions at the cell periphery is a sign of defects in focal adhesion dynamics, which are essential for cell movement (34−37). Vinculin was localized in those peripheral adhesions that turn over rapidly during cell spreading (38). The production and assembly of vinculin-positive focal adhesions are indicators of biocompatibility and stability for

cell behaviors such as adhesion, migration, growth, and differentiation. The results of the vinculin localization on N-HA (400 and 550) and P-HA (400 and 550) suggested that both of the polarized HA surfaces were suitable for the formation of focal complexes and subsequent focal adhesions. These benefits could contribute to cell behaviors on the polarized HA.

The mechanism of cell adhesion on biomaterials varied according to the type of substrate and depended on the kinds and amount of proteins previously adsorbed on the biomaterials (39, 40). Human osteoblast-like cells initially attached and spread more quickly on the HA surface than they did on titanium (1) because the molecules regulating cell spreading on HA, such as vitronectin and fibronectin, were apparently different from those on titanium (41). Furthermore, HA and titanium surfaces influence the gene expression of adhesion proteins early during adhesion as well as during the proliferation and differentiation phases (4). The signal transduction pathways involved in the adhesion of osteoblastic cells on HA and titanium were confirmed by the sequential expression of $\alpha_v\beta_1$ integrins, focal adhesion kinase (FAK), and extracellular signal-regulated kinase (ERK) genes followed by the expression of the c-jun and c-fos genes for proliferation and the alkaline phosphatase gene for differentiation (1). Mitogen-activated protein phosphorylation, spreading, and focal adhesion formation were enhanced on Ti6Al4V and FN-coated glass compared with poly($_L$-lysine)-coated glass (42). These effects on the signal transduction pathway through the adsorbed proteins on the various types of substrates resembled the effects detected on the polarized HA surfaces. N-HA and P-HA accelerated the adsorption of fibrin that is one of the cell adhesion proteins (19). This acceleration of the protein adsorption has a chance to be effective on cell adhesion through the signal transduction. In comparison with other biomaterials, the surface wettability of HA had advantages for protein adsorption (43). One of the important reasons for the enhancement of cell spreading on N-HA and P-HA is certainly the improved surface wettability. The decrease of the contact angle was induced from the high surface energy, which supported high protein adsorption on the substrate surface (27, 30). The high adsorbed proteins, especially cell adhesion proteins, contribute to cell adhesion and spreading.

In conclusion, this study provides two new and important items of information on polarized HA surface characteristics and cell behavior on polarized HA. First, polarization improved the wettability of the HA surface. Furthermore, the stored charges on the HA induced by the polarization were maintained during sterilization with ethanol and cell cultivation. Second, the improvement of the surface wettability, consequently, affected osteoblastic adhesion, especially spreading.

Acknowledgment. This work was partly supported by Grants-in-Aid from the Japan Society for the Promotion of Science (No. 19300169 and No. 21700485) and the Kazuchika Okura Memorial Foundation. Gratitude is expressed to Miyuki Soga and Tomoko Soya for technical assistance.

REFERENCES AND NOTES

(1) Okumura, A.; Goto, M.; Goto, T.; Yoshinari, M.; Masuko, S.; Katsuki, T.; Tanaka, T.*Biomaterials* **2001**, *22* (16), 2263–2271.
(2) Lampin, M.; Warocquier-Clerout, R.; Legris, C.; Degrange, M.; Sigot-Luizard, M. F.*J. Biomed. Mater. Res.* **1997**, *36* (1), 99–108.
(3) Advincula, M. C.; Rahemtulla, F. G.; Advincula, R. C.; Ada, E. T.; Lemons, J. E.; Bellis, S. L.*Biomaterials* **2006**, *27* (10), 2201–2212.
(4) Rouahi, M.; Champion, E.; Hardouin, P.; Anselme, K. *Biomaterials* **2006**, *27* (14), 2829–2844.
(5) Schwartz, Z.; Boyan, B. D. *J. Cell. Biochem.* **1994**, *56* (3), 340–347.
(6) Redey, S. A.; Nardin, M.; Bernache-Assolant, D.; Rey, C.; Delannoy, P.; Sedel, L.; Marie, P. J. *J. Biomed. Mater. Res.* **2000**, *50* (3), 353–364.
(7) Wang, Y.; Zhang, S.; Zeng, X.; Ma, L. L.; Khor, K. A.; Qian, M. *J. Biomed. Mater. Res., Part A* **2008**, *84* (3), 769–776.
(8) Aronov, D.; Karlov, A.; Rosenman, G. *J. Eur. Ceram. Soc.* **2007**, *27*, 4181–4186.
(9) Clark, E. A.; Brugge, J. S.*Science* **1995**, *268* (5208), 233–239.
(10) Miyamoto, S.; Teramoto, H.; Coso, O. A.; Gutkind, J. S.; Burbelo, P. D.; Akiyama, S. K.; Yamada, K. M. *J. Cell Biol.* **1995**, *131* (3), 791–805.
(11) Ben Ze'ev, A.; Farmer, S. R.; Penman, S. *Cell* **1980**, *21* (2), 365–372.
(12) Yamashita, K.; Oikawa, N.; Umegaki, T. *Chem. Mater.* **1996**, *8* (12), 2697–2700.
(13) Yamashita, K.; Nakamura, S. *J. Ceram. Soc. Jpn.* **2005**, *113*, 1–9.
(14) Ueshima, M.; Nakamura, S.; Yamashita, K. *Adv. Mater.* **2002**, *14* (8), 591–593.
(15) Nakamura, S.; Takeda, H.; Yamashita, K. *J. Appl. Phys.* **2001**, *89* (10), 5386–5392.
(16) Iwasaki, T.; Tanaka, Y.; Nakamura, M.; Nagai, A.; Katayama, K.; Yamashita, K. *J. Ceram. Soc. Jpn.* **2008**, *116*, 23–27.
(17) Kobayashi, T.; Nakamura, S.; Yamashita, K. *J. Biomed. Mater. Res.* **2001**, *57* (4), 477–484.
(18) Itoh, S.; Nakamura, S.; Nakamura, M.; Shinomiya, K.; Yamashita, K. *Biomaterials* **2006**, *27*, 5572–5579.
(19) Nakamura, M.; Nakamura, S.; Sekijima, Y.; Niwa, K.; Kobayashi, T.; Yamashita, K. *J. Biomed. Mater. Res. A* **2006**, *79* (3), 627–634.
(20) Nagai, A.; Yamashita, K.; Imamura, M.; Azuma, H. *Life Sci.* **2008**, *82* (23–24), 1162–1168.
(21) Okabayashi, R.; Nakamura, M.; Okabayashi, T.; Tanaka, Y.; Nagai, A.; Yamashita, K. *J. Biomed. Mater. Res., Part B* **2009**, *90*, 641–646.
(22) Nakamura, M.; Nagai, A.; Tanaka, Y.; Sekijima, Y.; Yamashita, K. *J. Biomed. Mater. Res., Part A* **2009**, in press.
(23) Valta, M. P.; Hentunen, T.; Qu, Q.; Valve, E. M.; Harjula, A.; Seppanen, J. A.; Vaananen, H. K.; Harkonen, P. L. *Endocrinology* **2006**, *147* (5), 2171–2182.
(24) Kato, S.; Kidoaki, S.; Matsuda, T. *J. Biomed. Mater. Res., Part A* **2004**, *68* (2), 314–324.
(25) Lu, H. B.; Campbell, C. T.; Graham, D. J.; Ratner, B. D. *Anal. Chem.* **2000**, *72*, 2886–2894.
(26) Xu, L. C.; Shiedlecki, C. A. *Biomaterials* **2007**, *28* (22), 3273–3283.
(27) Webb, K.; Hlady, V.; Tresco, P. A. *J. Biomed. Mater. Res.* **1998**, *41* (3), 422–430.
(28) Hao, L.; Lawrence, J.; Chian, K. S. *J. Mater. Sci.: Mater. Med.* **2005**, *16* (8), 719–726.
(29) Das, K.; Bose, S.; Bandyopadhyay, A. *Acta Biomater.* **2007**, *3* (4), 573–585.
(30) Lim, J. Y.; Shaughnessy, M. C.; Zhou, Z.; Noh, H.; Vogler, E. A.; Donahue, H. J. *Biomaterials* **2008**, *29* (12), 1776–1784.
(31) Deligianni, D. D.; Katsala, N. D.; Koutsoukos, P. G.; Missirlis, Y. F. *Biomaterials* **2001**, *22* (1), 87–96.
(32) Zaidel-Bar, R.; Ballestrem, C.; Kam, Z.; Geiger, B. *J. Cell Sci.* **2003**, *116* (22), 4605–4613.
(33) Berrier, A. L.; Yamada, K. M. *J. Cell. Physiol.* **2007**, *213* (3), 565–573.

(34) Saunders, R. M.; Holt, M. R.; Jennings, L.; Sutton, D. H.; Barsukov, I. L.; Bobkov, A.; Liddington, R. C.; Adamson, E. A.; Dunn, G. A.; Critchley, D. R. *Eur. J. Cell Biol.* **2006**, *85* (6), 487–500.
(35) Burridge, K.; Chrzanowska-Wodnicka, M. *Annu. Rev. Cell Dev. Biol.* **1996**, *12*, 463–519.
(36) Wu, X.; Kodama, A.; Fuchs, E. *Cell* **2008**, *135* (1), 137–148.
(37) Schrock, Y.; Solis, G. P.; Stuermer, C. A. *FEBS Lett.* **2009**, *583* (2), 389–393.
(38) Ziegler, W. H.; Liddington, R. C.; Critchley, D. R. *Trends Cell Biol.* **2006**, *16* (9), 453–460.
(39) Kilpadi, K. L.; Sawyer, A. A.; Prince, C. W.; Chang, P. L.; Bellis, S. L. *J. Biomed. Mater. Res., Part A* **2004**, *68* (2), 273–285.
(40) Masiello, L. M.; Fotos, J. S.; Galileo, D. S.; Karin, N. J. *Bone* **2006**, *39* (1), 72–82.
(41) Matsuura, T.; Hosokawa, R.; Okamoto, K.; Kimoto, T.; Akagawa, Y. *Biomaterials* **2000**, *21* (11), 1121–1127.
(42) Krause, A.; Cowles, E. A.; Gronowicz, G. *J. Biomed. Mater. Res.* **2000**, *52* (4), 738–747.
(43) Matsumura, H.; Kawasaki, K.; Okumura, N.; Kambara, M.; Norde, W. *Colloids Surf. B* **2003**, *32* (2), 97–103.

AM900341V